Optical Properties of a Nanosized Hole in a Thin Metallic Film

Tae-Ho Park,[†] Nikolay Mirin,[‡] J. Britt Lassiter,[†] Colleen L. Nehl,[†] Naomi J. Halas,[‡,§] and Peter Nordlander[†,§,*]

[†]Department of Physics and Astronomy, M.S. 61, [‡]Department of Chemistry, M.S. 60, [§]Department of Electrical and Computer Engineering, M.S. 366, and Laboratory for Nanophotonics, Rice University, Houston, Texas 77005-1892

ABSTRACT Subwavelength holes are one of the most important structures in nanophotonics, providing a useful geometry for nanosensing and giving rise to extraordinary transmission when patterned in arrays. Here we theoretically and experimentally examine the optical properties of an individual nanohole in a thin metallic film. In contrast to localized plasmonic nanostructures with their own characteristic resonances, nanoholes provide a site for excitation of the underlying thin film surface plasmons. We show that both hole diameter and film thickness determine the energy of the optical resonance. A theoretical dispersion curve was obtained and verified using spectral measurements of individual nanoholes.

The optical properties of metallic nanostructures are a subject of considerable fundamental and technological importance. The excitation spectrum of a metallic nanostructure is determined by its plasmon resonances, which are collective oscillations of the conduction electrons. The energies of plasmon resonances can depend strongly on shape and composition of the nanostructure.[1–7] Examples of highly tunable plasmonic nanoparticles are metallic nanoshells[8] and nanorods.[9,10] The tunability of the plasmon resonances of metallic nanoparticles can be exploited to position the optical resonances at specific wavelength regions of interest and has led to a wide range of applications across many disciplines in science and engineering. In addition to their fundamental importance, plasmonic nanostructures are receiving a great deal of attention for their potential applications in areas such as subwavelength waveguiding,[11,12] substrates for surface-enhanced spectroscopies,[13–16] sensing, biotechnology, and biomedicine.[17–20] The development of novel synthesis methods for nanostructure fabrication[21–24] and new theoretical approaches for the understanding of their optical properties[25–30] is making the field of nanophotonics an area of intense current interest.

Among various metallic nanostructures, a nanosized aperture, or nanohole, in a thin metal film has received particular attention since the discovery of the extraordinary optical transmission (EOT) phenomenon in nanohole arrays.[31–33] Near-field optical experiments have provided clues toward understanding this effect,[34–36] but the underlying physical mechanisms for enhanced transmission are not yet fully clarified.[37–39]

In order to fully understand the properties of complex systems such as nanohole arrays and single nanoholes of complex shape, one must first understand the most basic system, a single circular aperture in a thin metallic film. The optical properties of a single nanohole have been previously studied experimentally by other groups. The measured elastic scattering spectra have revealed that a hole plasmon resonance (HPR) is tuned to longer wavelengths by increasing the diameter of the hole.[40,41] Near-field scanning optical microscopy (NSOM) experiments have shown that the hole acts as a scattering center for surface plasmon polaritons (SPPs).[35,41] In the optical response of isolated holes, it has also been shown that the HPR wavelength is sensitive to its local dielectric environment and that the nanohole is useful for chemical and biological sensing applications.[40,42,43] Several studies of the optical properties of individual nanoholes in metallic films have been performed using numerical approaches with results that agree well with experimental findings. Finite-difference time-domain (FDTD) simulations have been used to elucidate the origins of fringe patterns in films arising from the near field of a single nanohole,[35,44] and the dependence of hole size and local dielectric environment on the light transmission and field

*Address correspondence to nordland@rice.edu.

Received for review October 10, 2007 and accepted December 06, 2007.

Published online January 9, 2008.
10.1021/nn700292y CCC: $40.75

enhancement of nanohole systems has been shown.[45] Boundary element method (BEM) has also been shown to reproduce the red shifts of HPRs with increasing hole diameter using transmission calculations.[41] Other methods such as the multiple multipole (MMP) technique[46] and analytic calculations based on a normal-mode-decomposition technique[47] have shown that SPPs strongly enhance the light scattering with subwavelength apertures in a metallic thin film. However, a clear picture of the microscopic origin of the HPR and the strong dependence of its energy on hole size has not yet emerged.

In this paper, we provide a simple and physically intuitive picture of the HPR in a thin metallic film. In the thin film limit, the plasmons become symmetric and antisymmetric linear combinations of propagating surface plasmons localized on the upper and lower surfaces of the metal. In this case, the plasmon dispersion depends strongly on the thickness of the film.[48] Using the plasmon hybridization (PH) method, we show that the dispersion relations of the plasmon modes of a thin metallic film with a hole are the same as those of a continuous film. When the hole is present, the film plasmons can induce charges along the surface of the hole. Plasmon modes of corresponding spatial wavelengths can thus induce a dipole moment across the hole. These film plasmons, exposed by the presence of the hole, become optically active and can be directly excited in contrast to the surface plasmon waves of a continuous film, which require evanescent excitation.[48] It is these film plasmons rather than a localized hole-induced plasmon resonance that constitutes the HPR. Since the energies of thin film plasmons also depend on the thickness of the film, the energy of the HPR will also depend on film thickness. We verify this by measuring the scattering spectra of holes of fixed diameter in metallic films of varying thicknesses. To our knowledge, the film thickness dependence of the HPR has not been previously examined either experimentally or theoretically.

RESULTS AND DISCUSSION

To understand the physical mechanism of the HPR, we start by analyzing the plasmonic properties and optical absorption of a hole in a thin perfect metallic film in a vacuum, using a simple approach that neglects retardation effects. This analysis provides a simple and intuitive explanation of the microscopic origin of the HPR. Specifically, it predicts that for a fixed hole diameter, the energy of the HPR can be tuned by changing the thickness of the metallic film. The insight obtained from this simple model can then be used to analyze the optical properties of a more realistic system, that is, a nanosized hole in a metallic film deposited on a substrate, modeled using realistic dielectric data and including retardation effects. Finally, our experimental study shows that the HPR can be tuned by changing the film thickness while keeping the hole diameter fixed.

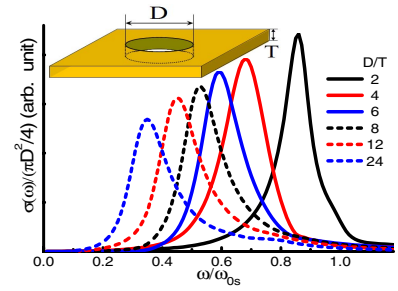

Figure 1. Dipolar optical absorption spectra of the hole/film system calculated by the plasmon hybridization (PH) method for different aspect ratios, that is, the ratio of the diameter of the hole and the film thickness (*D*/*T*) probed by parallel polarization of incident light. The spectra are normalized by hole area. The aspect ratios are listed, in the key to the right, with color and line style corresponding to the respective spectrum. In the top inset, the geometrical structure for our calculation is displayed.

In the Methods section, we use the PH method[49] to derive the film plasmon dispersion relation and an expression for the optical spectra of a hole of diameter *D* in a thin metallic film of thickness *T*. We show that the dispersion of film plasmons is unaffected by the presence of an individual hole. In an electrostatic approach such as the PH method, the optical properties of a nanostructure are scale invariant and can only depend on the structural parameters of the system as the aspect ratio *D*/*T*. In Figure 1, we show the calculated absorption spectra for incident light perpendicular to the film for several different aspect ratios *D*/*T*. For a given aspect ratio, the spectrum is asymmetric and consists of a strong absorption feature at low energies, the HPR, and several weaker features at higher energies. The figure reveals a clear red shift of the HPR with increasing hole diameter.

In the PH method, the plasmon modes of the film are obtained as linear combinations of the surface plasmons associated with the upper and lower surfaces. The dispersion relation for the film plasmons is

$$\omega_{sp}(\vec{k},\pm) = \omega_S\sqrt{1 \pm \exp(-|\vec{k}|T)} \qquad (1)$$

where $\vec{k}$ is the two-dimensional propagation wavevector of the surface plasmon modes.[50] The $-$ sign denotes the bonding (B) film plasmon with symmetric alignment of surface charges on the top and bottom surfaces. The $+$ sign refers to the antibonding (AB) film plasmon with an opposite alignment of the surface charges. The charge alignment of the A and AB modes is illustrated in panels a and d in Figure 2. The surface plasmon frequency is defined as $\omega_S = (2\pi n_0 e^2/m_e)$ where n_0 is the conduction electron density and m_e is the effective mass of a conduction electron.

The physical mechanism for the excitation of the HPR is illustrated in Figure 2. In the dipole approxima-

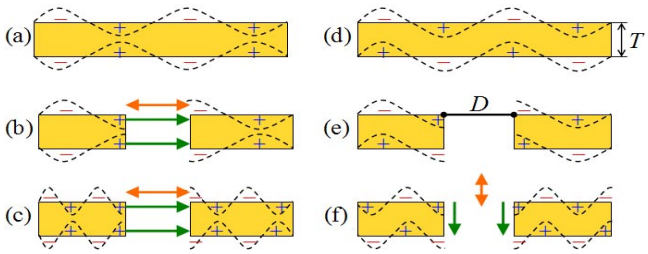

Figure 2. Charge configuration for bonding (B) and antibonding (AB) film plasmon modes and the mechanism by which a nanohole allows coupling of light to these modes: (a) symmetric charge modulation of B mode; (b) optimal coupling between a B film plasmon mode and light of parallel polarization; (c) coupling between a higher order B film plasmon mode and light of parallel polarization; (d) antisymmetric charge modulation of AB mode; (e) no coupling between any AB film plasmon mode and light of parallel polarization; (f) optimal coupling between an AB film plasmon mode and light of perpendicular polarization. Orange arrows represent the polarization direction of the incident light, and green arrows indicate the dipole moments resulting from the plasmon induced charges on the surfaces of the hole.

tion, the coupling of light with surface plasmons is proportional to the square of the dipole moment of the plasmons. For this reason, light polarized parallel to the surface can couple only to B film plasmons. (Perpendicularly polarized light can couple to AB plasmons as shown in Figure 2f.) On a continuous metallic surface, the plasmons possess no dipole moment. However, in the presence of a hole, the film plasmons can obtain a dipole moment due to the localized surface charges induced along the rim of the hole.

The optimal coupling between light polarized parallel to the surface occurs for film plasmons of half-wavelength equal to the diameter of the hole,

$$k_{sp}^{opt} \approx 0.83\pi/D \qquad (2)$$

The numerical factor 0.83 is due to the transformation of the wavevector of a plane wave in Cartesian coordinates into cylindrical coordinates (diffraction) and is equal to the ratio of the wavevector for which a sine wave is maximum and the wavevector for which a cylindrical Bessel function of order one is maximum. The microscopic nature of the HPR in the electrostatic limit is thus a superposition of film plasmons centered at the wavevector given by eq 2.

As a result, we can expect a strong HPR at an energy

$$\omega_{HPR} = \omega_{sp}(k_{sp}^{opt}) = \omega_S\sqrt{1-\exp(-0.83\frac{\pi T}{D})} \qquad (3)$$

This expression is in perfect agreement with the results in Figure 1 and shows clearly that the HPR will red shift both with increasing hole radius and with decreasing film thickness. While the red shift of the HPR with hole diameter is a simple geometric effect, the red shift with decreasing film thickness can be understood using simple electrostatics. For decreasing film thickness, the attractive electrostatic interaction between the surface charges on the opposite sides of the hole increases.

Larger wavevector surface plasmons can also induce localized dipole moments across the hole as illustrated in Figure 2c. The largest dipole moments are induced for plasmon wavelengths satisfying $k_{sp} = c_N(2N-1)\pi/D$ where N is an arbitrary integer and c_N are the corresponding diffraction coefficients. These higher order plasmons give rise to absorption features at higher energies. However, the intensities of these features are strongly suppressed since the effective interaction with the incident field decays as the square of the dipole moment of the film plasmon eq 16, that is, as $1/k^3$. Nonetheless, the spectra in Figure 1 clearly reveal weak absorption features at larger energies than the HPR.

A more realistic system consisting of a nanosized hole in a thin metallic film on top of a glass substrate is schematically illustrated in the inset of Figure 3b. To determine the energy of the HPR, we need to calculate the film plasmon dispersion relations including retardation effects and a realistic dielectric description of the materials.

For a metallic film on a substrate, the dispersion relations of the film plasmons can be calculated directly from the Maxwell equations in a planar geometry,[51,52]

$$\left(\frac{\epsilon_2}{\epsilon_1(\omega)}+\frac{\gamma_2(\omega)}{\gamma_1(\omega)}\right)\left(\frac{\epsilon_0}{\epsilon_1(\omega)}+\frac{\gamma_0(\omega)}{\gamma_1(\omega)}\right)e^{2\gamma_1(\omega)T} = \left(\frac{\epsilon_2}{\epsilon_1(\omega)}-\frac{\gamma_2(\omega)}{\gamma_1(\omega)}\right)\left(\frac{\epsilon_0}{\epsilon_1(\omega)}-\frac{\gamma_0(\omega)}{\gamma_1(\omega)}\right) \qquad (4)$$

where ϵ_i (i = 0, 1, 2) is the dielectric function in each region, that is, vacuum, Au, and glass, respectively. This expression includes retardation effects. To model the gold film $\epsilon_1(\omega)$, we use the Johnson and Christy (JC) data.[53] For the glass substrate, we use a constant dielectric permittivity of $\epsilon_2 = 2.25$. The quantities γ_i are the perpendicular components of the wavevector and have the form $\gamma_i^2 = k^2 - \epsilon_i(\omega/c)^2$. The dispersion relation can be obtained analytically by solving eq 4; the imaginary part of ϵ_1 does not affect this solution as long as surface plasmon oscillations remain weakly damped.[51] Figure 3a shows the dispersion relations of metallic films of several thicknesses supported by a glass substrate. To emphasize that these plasmons are calculated using a fully retarded approach, we refer to the energies of these modes as surface plasmon polariton modes (SPP) with energies $\omega_{spp}(k)$. As in the electrostatic limit, for each wavevector there are two SPP modes corresponding to a symmetric and antisymmetric alignment of the surface charges on the two

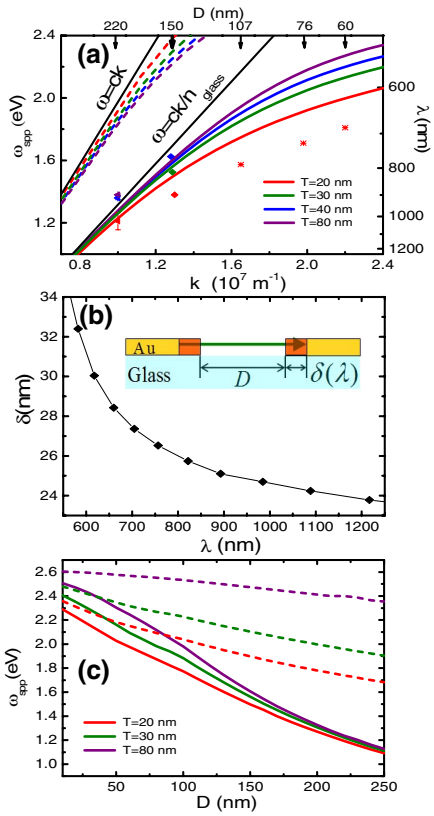

Figure 3. (a) Dispersion relations calculated using eq 4 for a nanohole in a thin metal film supported by a glass substrate for different film thicknesses: $T = 20$ nm (red), 30 nm (green), 40 nm (blue), and 80 nm (violet). The upper branches are the antibonding (AB) film plasmon modes, and the lower branches are the bonding (B) modes. Solid lines are bound modes, and dashed lines are leaky modes. The light lines for vacuum $\omega = ck$ and for glass $\omega = ck/n_{glass}$ are included as a guide to the eye. The HPR parameters deduced from the scattering spectra in Figure 4 are shown in symbols: (▲) $D = 220$ nm; (◆) $D = 150$ nm. The red stars denote the HPR parameters deduced from the experimental data for different D (scale on top of the figure) in ref 41. (b) Skin depth of Au ($\delta(\lambda)$) as a function of wavelength (λ) calculated using eq 5 and JC data. The inset shows an illustration of the penetration $\delta(\lambda)$ of the incident light. (c) Energies of HPR calculated using retarded (solid lines) and electrostatic (dashed lines) film plasmon dispersions as a function of hole diameter D and film thicknesses $T = 20$ nm (red), 30 nm (green), and 80 nm (violet).

surfaces of the film. For SPP modes in this geometry, the modes are classified as "bound" if the modes lie below the light line for glass and "leaky" if the modes lie below the light line for vacuum but above the light line for the glass substrate. For the small wavevectors shown in Figure 3a, the antibonding modes are "leaky", that is, bound at the metal/vacuum interface but radiative at the metal/glass substrate interface. For larger wavevectors, these antibonding modes lie below the glass light line and are therefore bound at both interfaces.[41,54]

For a realistic description of the interaction of light with a nanosized hole, we also need to include the penetration of light into the metal around the hole (Figure 3b, inset). This penetration increases the effective size of

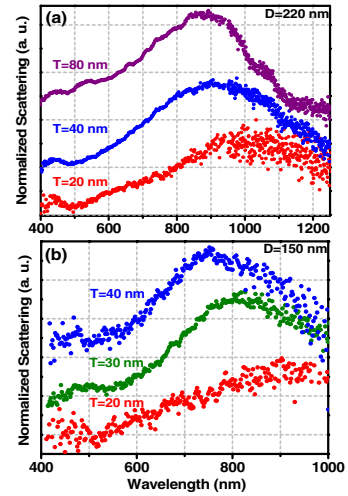

Figure 4. Experimental measurement of optical scattering for different hole/film systems: (a) individual nanoholes with diameter 220 nm and film thicknesses 80, 40, and 20 nm with corresponding peak positions at $\lambda_R = 897$, 912, and 1020 ± 54.6 nm; (b) individual nanoholes with diameter 150 nm and film thicknesses 40, 30, and 20 nm with corresponding peak positions at $\lambda_R = 755$, 815, and 900 nm. Except for the $T = 20$ nm and $D = 220$ nm hole, the standard deviations of λ_R are less than 1.5%.

the hole and alters the resonance condition of eq 2 obtained using the nonretarded PH method. A rigorous calculation of δ would require taking into account both quantum and cavity quantum electrodynamic effects. As a simple estimate of this effect, we assume that the penetration depth δ is equal to the conventional skin depth. For a planar geometry, the skin depth of a metal is equal to

$$\delta(\omega) = \frac{\sqrt{2}c}{\omega}\left(\sqrt{\epsilon_R(\omega)^2 + \epsilon_I(\omega)^2} - \epsilon_R(\omega)\right)^{-1/2} \qquad (5)$$

where $\epsilon_R(\omega)$ ($\epsilon_I(\omega)$) is the real (imaginary) part of the dielectric function, ω is the angular frequency of the light, and c is the speed of light. The skin depth, $\delta(\omega)$, for Au, calculated using JC data, is plotted as a function of wavelength in Figure 3b. The graph shows that in the near-infrared (NIR) light can penetrate the Au by as much as 20−35 nm. With the penetration depth included, the optimal coupling occurs for film SPP modes of wavevectors centered around

$$k_{spp}^{opt} = 0.83\frac{\pi}{D + 2\delta(\omega_{HPR})} \qquad (6)$$

where $\omega_{HPR} = \omega_{spp}(k_{spp}^{opt})$. This equation predicts that the energy of the HPR can be directly obtained from the dispersion relation for the film SPP modes. We will refer to the parameters (k_{spp}^{opt}, ω_{HPR}) as the HPR parameters. Using this approach, we can now analyze results from a recent study of the effect of hole diameter, D, on the HPR of a hole in a Au film of thickness $T = 20$ nm.[41] The energies of this HPR measurements, along with our prediction for the SPP wavevector eq 6, are shown

in Figure 3a. The HPR parameters follow the dispersion curve well and provide support for our simple model for the excitation mechanism of the HPR. The deviations from the experimental data may be due to material parameters or our oversimplified expression for the penetration depth δ or because the fabricated holes are not perfectly cylindrical. In this previous study, they also directly measured a wavelength $\lambda_{spp} \approx 285$ nm of the SPP mode excited by 633 nm laser light for a $D = 60$ nm diameter hole. This result is in good agreement with eq 6, which predicts $k_{spp}^{opt} \approx 2.2 \times 10^7$ m^{-1} corresponding to a wavelength of 280 nm.

In Figure 3c, we show the energy of the HPR as a function of hole diameter and film thickness. The figure directly shows the tunability of the HPR with these parameters. For comparison, we also show the results calculated using film plasmon dispersions determined using an electrostatic approach neglecting retardation. The effect of retardation is a red shift of the long wavelength film plasmons. This red shift results in a stronger dispersion of the film plasmon and thus a stronger dependence of the energy of the HPR on hole diameter. Retardation effects also decrease the coupling of the plasmon-induced charges on the opposite surfaces of the film leading to a reduced film thickness dependence of the long wavelength bonding film plasmon modes. This is why the retarded calculation gives a weaker thickness dependence of the HPR compared with the nonretarded calculation.

Figure 4 shows characteristic scattering spectra of individual holes of 220 and 150 nm diameter in Au films of varying thickness. These data clearly illustrate the predicted red shift of the HPR with decreasing film thickness. For $D = 220$ nm, the HPR shifts from 897 to 1020 nm when the thickness of the film changes from 80 to 20 nm. For $D = 150$ nm, the HPR red shifts from 755 to 900 nm as the thickness of the film is decreased from 40 to 20 nm. This figure also clearly shows the previously observed red shift of the HPR with hole diameter for constant film thickness.[40] As noted previously, the HPR spectra are significantly broader than individual nanoparticle spectra.[40,41] We believe that this is because a distribution of film SPP modes of wavevectors centered around the optimum film SPP wavevector k_{spp}^{opt} given by eq 6 can be excited. For an individual nanoparticle, only a distinct plasmon resonance is excited.

The energies of the HPR shown in Figure 4 along with the corresponding wavevectors obtained using eq 6 are shown in the dispersion relations in Figure 3a. The experimental data follow the theoretical predictions very well. For instance, not only does the HPR red shift with decreasing film thickness, but the magnitude of the shift is also smaller at higher energies, exactly as predicted by the dispersion relations. We also see the weak shoulders in the shorter wavelength (higher energy) region of the scattering spectra, which we believe may be due to excitation of higher order B modes. The experimental geometry also allows for the excitation of "leaky" antibonding film SPP modes, which should appear around 450 nm. These would be strongly damped due to interband transitions, which contribute below 500 nm. We believe that the small peak around 450 nm is most likely caused by interband transitions.

The present approach could in principle be extended to individual nanoholes of arbitrary shapes and to periodic hole arrays. For a single noncylindrical hole, our finding that the plasmons of the film were unaffected by the presence of the hole would still apply. However, the hole would introduce couplings between SPP modes of different azimuthal symmetries *m* leading to excitations of SPP modes centered around several different wavevectors rather than around a single wavevector such as the simple resonance condition eq 6. For a periodic array of holes, the film SPP dispersion would no longer be unaffected by the holes but would exhibit bandgaps and other features characteristic of periodic structures. The description of such effects and their influence on the electromagnetic properties of hole arrays is better handled using numerical approaches such as the finite-difference time-domain or finite element methods.

CONCLUSIONS

Using the plasmon hybridization approach, we have presented a simple physical explanation for the experimentally observed resonance in the optical spectra of nanosized holes in thin metallic films. When the hole is present, the film plasmons induce charges on the surfaces of the hole. Film plasmons of certain wavelengths that depend on the diameter of the hole can induce a large dipole moment across the hole. The hole thus mediates a coupling between these specific film plasmons and an incident electromagnetic wave. A simple expression for the wavelength of the dipole-active film plasmons is obtained. For increasing hole diameter, the wavelength of the dipole-active film plasmons increases resulting in a red-shifted energy of the hole resonance. Our approach provides a quantitative explanation for the experimentally observed red shift of a hole resonance as a function of hole diameter in previous experiments on films with fixed film thickness. We predict a red shift of the energy of the hole resonance with decreasing film thickness, which is substantiated in experimental measurements on individual nanoholes.

METHODS

Theory. In the electrostatic limit, the nanohole in a thin metallic film system can be treated analytically using the plasmon hybridization (PH) method.[49,50] The incompressible deformations of the electron gas in a film can be expressed in cylindrical coordinates (ρ, φ, and *z*), where the origin of the coordinate system is placed in the center of the hole with the *z*-axis perpendicular to the surface. The primitive plasmons of the system are obtained from the scalar potential, η

$$\eta = \frac{L^2}{(2\pi)^2}\sum_m \int \mathrm{d}k\, k[\dot{P}(k,m,t)J_m(k\rho)\mathrm{e}^{im\varphi}\mathrm{e}^{kz} + \dot{Q}(k,m,t)J_m(k\rho)\mathrm{e}^{im\varphi}\mathrm{e}^{-k(z+T)}] \quad (7)$$

where L^2 is the area of the film surface, and J_m is a cylindrical Bessel function of order *m*. The quantities $\dot{P}(k,m,t)$ and $\dot{Q}(k,m,t)$ are the time derivatives of the primitive surface plasmon modes amplitudes of a wavevector *k* and azimuthal symmetry *m* associated with the upper and lower film surface. The hole does not need to be included in the expression for η but will be included when calculating the kinetic and electrostatic contributions to the energy.

The Lagrangian for the primitive plasmons of the hole/film system is diagonal in *m* and can be written as

$$L^m = \int \mathrm{d}k \int \mathrm{d}k'\, [T^{1,m}_{k,k'}(\dot{P}(k)\dot{P}(k') + \dot{Q}(k)\dot{Q}(k')) + T^{2,m}_{k,k'}(\dot{P}(k)\dot{Q}(k') + \dot{Q}(k)\dot{P}(k'))] - \omega_S{}^2[V^{1,m}_{k,k'}(P(k)P(k') + Q(k)Q(k')) + V^{2,m}_{k,k'}(P(k)Q(k') + Q(k)P(k'))] \quad (8)$$

The kinetic energy, $T_k k'^{i,m}$, and the interaction energy, $V_k k'^{i,m}$, terms represent the propagation and scattering of a film plasmon of a wavevector *k* into another wavevector *k*′, respectively. The kinetic energy terms can be written,

$$T^{1,m}_{k,k'} = \delta(k-k') + \kappa_1(k,k';a) + \kappa_3(k,k';a)$$
$$T^{2,m}_{k,k'} = \kappa_2(k,k';a) + \kappa_4(k,k';a) \quad (9)$$

where

$$\kappa_1(k,k';a) = \frac{k'\sinh\left(\frac{(k+k')T}{2}\right)}{(\sinh kT \sinh k'T)^{1/2}}\mathbb{J}_m(k,k';a) \quad (10)$$
$$\kappa_2(k,k';a) = \mathrm{e}^{kT}\kappa_1(k,k';a)$$
$$\kappa_3(k,k';a) = \frac{ak'}{k+k'}\kappa(k,k';a)$$
$$\kappa_4(k,k';a) = \frac{ak'}{k-k'}\kappa(k,k';a)$$
$$\kappa(k,k';a) = J_m(ka)J'_m(k'a)\frac{\sinh\left(\frac{(k+k')T}{2}\right)}{(\sinh kT \sinh k'T)^{1/2}}$$

where J'_m is the derivative of the Bessel function, and

$$\mathbb{J}_m(k,k';a) = \int_0^a \mathrm{d}\rho\, \rho J_m(k\rho)J_m(k'\rho) \quad (11)$$

for the hole with radius *a*.

The total interaction energy is calculated by evaluating the product of the electrostatic potential and the induced surface charges $\sigma(\vec{r})$ on all surfaces of the system.[49] The coefficients of the interaction energy take the form,

$$V^{1,m}_{k,k'} = \delta(k-k') - \gamma_0(k,k';a) - \gamma_0(k',k;a) + \gamma_1(k,k';a) + \gamma_3(k,k';a) \quad (12)$$
$$V^{2,m}_{k,k'} = -\mathrm{e}^{-kT}\delta(k-k') - \mathrm{e}^{-k'T}\gamma_0(k,k';a) + \mathrm{e}^{-kT}\gamma_0(k',k;a) - \gamma_2(k,k';a) + \gamma_3(k,k';a)$$

where

$$\gamma_0(k,k';a) = \frac{\sqrt{1-\mathrm{e}^{-2kT}}}{\sqrt{1-\mathrm{e}^{-2k'T}}}k'\mathbb{J}_m(k,k';a) \quad (13)$$
$$\gamma_1(k,k';a) = k'\int_0^\infty dp\, \mathbb{J}_m(p,k';a)\mathbb{J}_m(k,p;a) \frac{(1+\mathrm{e}^{-(k'+k)T}) - \mathrm{e}^{-pT}(\mathrm{e}^{-kT}+\mathrm{e}^{-k'T})}{\sqrt{(1-\mathrm{e}^{-2kT})(1-\mathrm{e}^{-2k'T})}}$$
$$\gamma_2(k,k';a) = k'\int_0^\infty dp\, \mathbb{J}_m(p,k';a)\mathbb{J}_m(k,p;a) \frac{\mathrm{e}^{-pT}(1+\mathrm{e}^{-(k'+k)T}) - (\mathrm{e}^{-kT}+\mathrm{e}^{-k'T})}{\sqrt{(1-\mathrm{e}^{-2kT})(1-\mathrm{e}^{-2k'T})}}$$
$$\gamma_3(k,k';a) = ak'\frac{(1-\mathrm{e}^{-k'T})J'_m(k'a)}{\sqrt{(1-\mathrm{e}^{-2kT})(1-\mathrm{e}^{-2k'T})}}\Big[(1-\mathrm{e}^{-2kT})J_m(ka) - k\int_0^\infty dp J_m(pa)\mathbb{J}_m(k,p;a)(1-\mathrm{e}^{-kT}-\mathrm{e}^{-pT}-\mathrm{e}^{-(p+k)T})\Big]$$

In the absence of the hole, only the delta functions $\delta(k-k')$ remain in eqs 9 and 12 and the Lagrangian becomes diagonal in *k* and *k*′.

To solve for the plasmon modes, the degrees of freedom *P*(*k*,*m*,*t*) and *Q*(*k*,*m*,*t*) defined in eq 7 are discretized in *k*-space. The Lagrangian is then converted to a quadratic form, which can be solved by application of the Euler–Lagrange equations. The calculated dispersion relations for the hole/film system take the form of eq 1 and are unaffected by the hole.

However, the presence of the hole has a pronounced effect on the optical spectra because an incident light wave can couple to the dipolar component of the surface charges induced by the plasmon modes around the hole. The interaction of an incident multipolar external field and plasmons of the nanohole system takes the form[49]

$$V^m_{\mathrm{I}} = \int \mathrm{d}S E_0(t) r^l Y_{lm}(\Omega)\sigma(\vec{r}) \quad (14)$$

where $E_0(t)$ is the time-dependent electric field, and $Y_{lm}(\Omega)$ are spherical harmonics. In the dipolar limit for parallel polarization, one only needs to consider $l = 1$, and $m = \pm 1$. The surface integral (dipole moment) of eq 14 is calculated in the same way as for the kinetic and potential energy calculation and results in

$$V^{\pm 1}_{\mathrm{I}} = \int \mathrm{d}k D(k)(P(k,\pm 1) + Q(k,\pm 1)) \quad (15)$$

where the dipolar couplings to the primitive film plasmons are

$$D(k) = Ca^2(1-\mathrm{e}^{-kT})(J_2(ka) + J'_1(ka)) \quad (16)$$

and *C* is a normalization constant. The frequency-dependent dipolar polarizability is given by

$$\alpha(\omega) = \int \mathrm{d}S r Y^*_{l=1,m}(\Omega)\sigma(\vec{r}) \quad (17)$$

and the optical absorption spectrum is obtained by taking the imaginary part of the polarizability as $\sigma(\omega) = (\omega/c)\mathrm{Im}[\alpha(\omega + i\delta)]$, where the broadening parameter δ is proportional to the imaginary part of the dielectric function of the metal. The probability for excitation of a plasmon mode is proportional to the square of its dipole moment, *D*(*k*).[55] For large *k*, the dipole moment *D*(*k*) vanishes as $1/k^{1.5}$ resulting in an effective incident light−plasmon coupling, which decreases as $1/k^3$. To calculate the optical absorption, the interaction term eq 15 is expressed in our discrete basis and added to the Lagrangian, which is then solved using matrix inversion.[49]

Experiments. The method for experimentally fabricating nanoholes is explained in detail elsewhere.[40] Briefly, polystyrene

spheres of a chosen diameter (desired diameter of nanoholes) are dispersed in a submonolayer onto a polydiallyldimethylammonium chloride (PDDA) functionalized glass slide. A Au layer of chosen thickness (here 20, 30, 40, and 80 nm) is evaporated onto the slide. The polystyrene spheres are then removed from the surface by tape-stripping, leaving behind a random distribution of nanoholes in the Au film. Scattering spectra were obtained for individual nanoholes using dark-field microscopy.[40] A nanohole sample is brought into the focus of a 100× reflection dark-field objective (Zeiss). The image of the nanohole (a point source of light) is focused onto the slit of one of two imaging spectrometers (Acton, MicroSpec 2150i) selected by a beam splitter. One spectrometer is coupled to a CCD (Princeton Instruments, PhotonMax) for measurements at visible wavelengths, while the other spectrometer is coupled to a 1-D InGaAs array (Princeton Instruments, OMA V) for NIR measurements. Once the image of the nanohole is positioned in the slit of one of the spectrometers, a grating is shifted into place for spectral measurements. NIR and visible spectra were spliced during data processing. The spectra were corrected for the instrument's spectral efficiency using a white calibration standard (Edmund Optics), and a background spectrum of the Au surface, in the vicinity of the nanohole, was subtracted from each spectrum. Film thicknesses measured by atomic force microscopy (Nanonics MV2000) were found to agree closely with thicknesses measured during evaporation (Sharon Vacuum e-beam evaporator).

Acknowledgment. This work is supported by the U.S. Army Research Laboratory and the U.S. Army Research Office under Contract/Grant Number W911NF-04-1-0203, the Robert A. Welch Foundation under Grant C-1220 and C-1222, and NSF under Grants EEC-0304097 and ECS-0421108.

REFERENCES AND NOTES

1. Liu, H.; Genov, D. A.; Wu, D. M.; Liu, Y. M.; Liu, Z. W.; Sun, C.; Zhu, S. N.; Zhang, X. Magnetic Plasmon Hybridization and Optical Activity at Optical Frequencies in Metallic Nanostructures. *Phys. Rev. B* **2007**, *76*, 073101.
2. Cortie, M.; Ford, M. A Plasmon-Induced Current Loop in Gold Semi-Shells. *Nanotechnology* **2007**, *18*, 235704.
3. Zhu, J. Ellipsoidal Core-Shell Dielectric-Gold Nanostructure: Theoretical Study of the Tunable Surface Plasmon Resonance. *J. Nanosci. Nanotechnol.* **2007**, *7*, 1059–1064.
4. Jain, P. K.; Huang, W.; El-Sayed, M. A. On the Universal Scaling Behaviour of the Distance Decay of Plasmon Coupling in Metal Nanoparticle Pairs: A Plasmon Ruler Equation. *Nano Lett.* **2007**, *7*, 2080–2088.
5. Wang, H.; Brandl, D. W.; Nordlander, P.; Halas, N. J. Plasmonic Nanostructures: Artificial Molecules. *Acc. Chem. Res.* **2007**, *40*, 53–62.
6. Guo, G.; Liu, N.; Fu, L.; Meyrath, T. P.; Zentgraf, T.; Schweizer, H.; Giessen, H. Resonance Hybridization in Double Split-Ring Resonator Metamaterials. *Opt. Express* **2007**, *15*, 12095–12101.
7. Wang, S.; Pile, D. F. P.; Sun, C.; Zhang, X. Nanopin Plasmonic Resonator Array and its Optical Properties. *Nano Lett.* **2007**, *7*, 1076–1080.
8. Halas, N. J. Playing with Plasmons: Tuning the Optical Resonant Properties of Metallic Nanoshells. *MRS Bull.* **2005**, *30*, 362–367.
9. Link, S.; El-Sayed, M. A. Spectral Properties and Relaxation Dynamics of Surface Plasmon Electronic Oscillations in Gold and Silver Nanodots and Nanorods. *J. Phys. Chem. B* **1999**, *103*, 8410–8426.
10. Murphy, C. J.; San, T. K.; Orendorff, C. J.; Gao, J. X.; Gou, L.; Hunyadi, S. E.; Li, T. Anisotropic Metal Nanoparticles: Synthesis, Assembly, and Optical Applications. *J. Phys. Chem. B* **2005**, *109*, 13857–13870.
11. Maier, S. A.; Kik, P. G.; Atwater, H. A.; Meltzer, S.; Harel, E.; Koel, B. E.; Requicha, A. G. Local Detection of Electromagnetic Energy Transport below the Diffraction Limit in Metal Nanoparticle Plasmon Waveguides. *Nat. Mater.* **2003**, *2*, 229–232.
12. Krenn, J. R.; Lamprecht, B.; Ditlbacher, H.; Schider, G.; Salerno, M.; Leitner, A.; Aussenegg, F. R. Non-Diffraction-Limited Light Transport by Gold Nanowires. *Europhys. Lett.* **2002**, *60*, 663–669.
13. Wei, G.; Wang, L.; Sun, L.; Song, Y.; Sun, Y.; Guo, C.; Yang, T.; Li, Z. Type I Collagen Mediated Synthesis and Assembly of UV Photoreduced Gold Nanoparticles and their Application in Surface Enhanced Raman Scattering. *J. Phys. Chem. C* **2007**, *111*, 1976–1982.
14. Aizpurua, J.; Bryant, G. W.; Richter, L. J.; de Abajo, F. J. G. Optical Properties of Coupled Metallic Nanorods for Field-Enhanced Spectroscopy. *Phys. Rev. B* **2005**, *71*, 235420.
15. Zhang, J.; Chowdhury, M. H.; Lakowicz, J. R. Metal-Enhanced Single-Molecule Fluorescence on Silver Particle Monomer and Dimer: Coupling Effect between Metal Particles. *Nano Lett.* **2007**, *7*, 2101–2107.
16. Bruzzone, S.; Malvaldi, M.; Arrighini, G. P.; Guidotti, C. SERS Effect in CO Physisorbed on Homogeneous and Core-Shell Nanoparticle Aggregates. *Theor. Chem. Acc.* **2007**, *118*, 67–73.
17. Khlebtsov, B. N.; Khlebtsov, N. G. Biosensing Potential of Silica/Gold Nanoshells: Sensitivity of Plasmon Resonance to the Local Dielectric Environment. *J. Quant. Spectrosc. Radiat. Transfer* **2007**, *106*, 154–169.
18. Larsson, E. M.; Alegret, J.; Kall, M.; Sutherland, D. S. Sensing Characteristics of NIR Localized Surface Plasmon Resonances in Gold Nanorings for Application as Ultrasensitive Biosensors. *Nano Lett.* **2007**, *7*, 1256–1263.
19. Saini, S.; Bhowmick, S.; Shenoy, V. B.; Bagchi, B. Rate of Excitation Energy Transfer Between Fluorescent Dyes and Nanoparticles. *J. Photochem. Photobiol. A* **2007**, *190*, 335–341.
20. Swathi, R. S.; Sebastian, K. L. Resonance Energy Transfer from a Fluorescent Dye Molecule to Plasmon and Electron-Hole Excitations of a Metal Nanoparticle. *J. Chem. Phys.* **2007**, *126*, 234701.
21. Peterson, M. S. M.; Bouwman, J.; Chen, A.; Deutch, M. Inorganic Metallodielectric Materials Fabricated using two Single-Step Methods based on the Tollen's Process. *J. Colloid Interface Sci.* **2007**, *306*, 41–49.
22. Ahrach, H. I. E.; Bachelot, R.; Vial, A.; Lerondel, G.; Plain, J.; Royer, P. Spectral Degeneracy Breaking of the Plasmon Resonance of Single Metal Nanoparticles by Nanoscale Near-Field Photopolymerization. *Phys. Rev. Lett.* **2007**, *98*, 107402.
23. Choi, B.-H.; Lee, H.-H.; Jin, S.; Chun, S.; Kim, S.-H. Characterization of the Optical Properties of Silver Nanoparticle Films. *Nanotechnology* **2007**, *18*, 075706.
24. Atanasov, P. A.; Takada, H.; Nedyalkov, N. N.; Obara, M. Nanohole Processing on Silicon Substrate by Femtosecond Laser Pulse with Localized Surface Plasmon Polariton. *Appl. Surf. Sci.* **2007**, *253*, 8304–8308.
25. Chern, R. L.; Liu, X. X.; Chang, C. C. Particle Plasmons of Metal Nanospheres: Application of Multiple Scattering Approach. *Phys. Rev. E* **2007**, *76*, 016609.
26. Romero, I.; Aizpurua, J.; Bryant, G. W.; de Abajo, F. J. G. Plasmons in Nearly Touching Metallic Nanoparticles: Singular Response in the Limit of Touching Dimers. *Opt. Express* **2006**, *14*, 9988–9999.
27. Papanikolau, N. Optical Properties of Metallic Nanoparticle Arrays on a Thin Metallic Film. *Phys. Rev. B* **2007**, *75*, 235426.
28. Jain, P. K.; El-Sayed, M. A. Universal Scaling of Plasmon Coupling in Metal Nanostructures: Extension from Nanoparticle Pairs to Nanoshells. *Nano Lett.* **2007**, *7*, 2854–2858.
29. Kaminski, F.; Sandoghdar, V.; Agio, M. Finite-Difference Time-Domain Modeling of Decay Rates in the Near Field of Metal Nanostructures. *J. Comput. Theor. Nanosci.* **2007**, *4*, 635–643.
30. Wang, S. M.; Xiao, J. J.; Yu, K. W. Tunable Coupled Plasmon Modes via Nanoshell Particle Chains. *Opt. Commun.* **2007**, *279*, 384–389.

31. Ebbeson, T. W.; Lezec, H. J.; Ghaemi, H. F.; Thio, T.; Wolf, P. A. Extraordinary Optical Transmission Through Sub-Wavelength Hole Arrays. *Nature* **1998**, *391*, 667–669.
32. de Abajo, F. J. G. Colloqium: Light Scattering by Particles and Hole Arrays. *Rev. Mod. Phys.* **2007**, *79*, 1267–1290.
33. Henzie, J.; Lee, M. H.; Odom, T. W. Multiscale Patterning of Plasmonic Metamaterials. *Nat. Nanotechnol.* **2007**, *2*, 549–554.
34. Gao, H.; Henzie, J.; Odom, T. W. Direct Evidence for Surface Plasmon-Mediated Enhanced Light Transmission Trough Metallic Nanohole Arrays. *Nano Lett.* **2006**, *6*, 2104–2108.
35. Yin, L.; Vlasko-Vlasov, V. K.; Rydh, A.; Pearson, J.; Welp, U.; Chang, S.-H.; Gray, S. K.; Schatz, G. C.; Brown, D. B.; Kimball, C. W. Surface Plasmons at Single Nanoholes in Au Films. *Appl. Phys. Lett.* **2004**, *85*, 467–469.
36. Korobkin, D.; Urzumov, Y. A.; Neuner, B.; Norman, C.; Zhang, Z.; Mayergoyz, I. D.; Shvets, G. Mid-Infrared Metamaterials based on Perforated SiC Membrane: Engineering Optical Response using Surface Phonon Polaritons. *Appl. Phys. A: Mater. Sci. Process.* **2007**, *88*, 605–609.
37. Gay, G.; Alloschery, O.; de Lesegno, B. V.; O'Dwyer, C. O.; Weiner, J.; Lezec, H. J. The Optical Response of Nanostructured Surfaces and the Composite Diffracted Wave Model. *Nat. Phys.* **2006**, *2*, 262–267.
38. Lezec, H. J.; Thio, T. Diffracted Evanescent Wave Model for Enhanced and Supressed Optical Transmission through Subwavelength Hole Arrays. *Opt. Express* **2004**, *12*, 3629–3651.
39. Kovarz, M. W. Homogeneous and Evanescent Contributions in Scalar Near-Field Diffraction. *Appl. Opt.* **1995**, *34*, 3055–3063.
40. Prikulis, J.; Hanarp, P.; Olofsson, L.; Sutherland, D. S.; Kall, M. Optical Spectroscopy of Nanometric Holes in Thin Gold Films. *Nano Lett.* **2004**, *4*, 1003–1007.
41. Rindzevicius, T.; Alaverdyan, Y.; Sepulveda, B.; Pakizeh, T.; Kall, M.; Hillenbrand, R.; Aizpurua, J.; de Abajo, F. J. G. Nanohole Plasmons in Optically Thin Films. *J. Phys. Chem. C* **2007**, *111*, 1207–1212.
42. Rindzevicius, T.; Alaverdyan, Y.; Dahlin, A.; Hook, F.; Sutherland, D. S.; Kall, M. Plasmonic Sensing Characteristics of Single Nanometric Holes. *Nano Lett.* **2005**, *5*, 2335–2339.
43. Dahlin, A.; Zach, M.; Rindzevicius, T.; Kall, M.; Sutherland, D. S.; Hook, F. Localized Surface Plasmon Resonance Sensing of Lipid-Membrane Mediated Biorecognition Events. *J. Am. Chem. Soc.* **2005**, *127*, 5043–5048.
44. Chang, S. H.; Gray, S. K.; Schatz, G. C. Surface Plasmon Generation and Light Transmission by Isolated Nanoholes and Arrays of Nanoholes in Thin Films. *Opt. Express* **2005**, *13*, 3150–3165.
45. Shuford, K. L.; Gray, S. K.; Ratner, M. A.; Schatz, G. C. Substrate Effect on Surface Plasmons in Single Nanoholes. *Chem. Phys. Lett.* **2007**, *435*, 123–126.
46. Wannemacher, R. Plasmon-Supported Transmission of Light through Nanometric Holes in Metallic Thin Films. *Opt. Commun.* **2001**, *195*, 107–118.
47. Lalanne, P.; Hugonin, J. P.; Rodier, J. C. Theory of Surface Plasmon Generation at Nanoslit Apertures. *Phys. Rev. Lett.* **2005**, *95*, 263902.
48. Raether, H. *Surface Plasmons on Smooth and Rough Surfaces and on Gratings*; Springer-Verlag: Berlin, 1988.
49. Prodan, E.; Nordlander, P. Plasmon Hybridization in Spherical Nanoparticles. *J. Chem. Phys.* **2004**, *120*, 5444–5454.
50. Le, F.; Zwin, N. Z.; Halas, N. J.; Nordlander, P. Plasmonic Interaction between a Metallic Nanoshell and a Thin Metallic Film. *Phys. Rev. B* **2007**, *76*, 165410.
51. Economou, E. N. Surface Plasmons in Thin Films. *Phys. Rev.* **1969**, *182*, 539–554.
52. Sernelius, B. E. *Surface Modes in Physics*; Wiley-VCH: Berlin,2001.
53. Johnson, P. B.; Christy, R. W. Optical Constants of the Noble Metals. *Phys. Rev. B* **1972**, *6*, 4370–4379.
54. Burke, J. J.; Stegeman, G. I.; Tamir, T. Surface-Polariton-Like Waves Guided by Thin Lossy Metal Films. *Phys. Rev. B* **1986**, *33*, 5186–5201.
55. Brandl, D. W.; Nordlander, P. Plasmon Modes of Curvilinear Metallic Core/Shell Particles. *J. Chem. Phys.* **2007**, *126*, 144708.